

Invitation to the 2015 “Blind test 4” Workshop

Combined power output of two in-line turbines at different inflow conditions

Lars Sætran and Jan Bartl

Department of Energy and Process Engineering, NTNU, Trondheim, Norway
Contact: lars.satran@ntnu.no, jan.bartl@ntnu.no

Abstract:

This note describes a 4th blind test case organized by NOWITECH and NORCOWE.

We invite you to submit predictions for the described test cases and participate in a two-day workshop to be held in Trondheim, scheduled for October 2015. Here, the results from the predictions will be discussed and a comparison with measurements will be presented.

Schedule:

- March 27th, 2015: Blind test invitation sent out
- Oct. 1st, 2015: Deadline for submission of simulation results
- End of Oct, 2015: Blind test workshop in Trondheim (you will be informed about the exact dates later)

Background:

BT1: The first blind test, BT1, was organized in Bergen, in October 2011, and attracted around 40 participants with 11 sets of predictions being submitted. For that blind test the geometry of a model turbine was made available and the participants were asked to predict its performance and the wake development from the turbine down to 5 diameters. The results from BT1 have been reported in [1].

BT2: For the next blind test, held in Trondheim, in October 2012, the test complexity was increased by adding a downstream turbine behind the upstream turbine. The main task in BT2 was to predict the performance of the downstream turbine, which is affected by the wake developing behind the upstream turbine. The participants were also asked to predict the flow in the wake behind the downstream turbine. Obviously, this was a more complicated test case than BT1 and required more computer resources to be performed properly. Despite this, results were submitted by 9 different participants. The results were reported in [2].

BT3: For the third blind test, BT3, the complexity was slightly increased again. The same turbines were used, positioned with the same streamwise separation, but shifted slightly sideways so that the wake from the upstream turbine only hit a part of the rotor plane of the downstream turbine. In this way the downstream turbine experienced an asymmetric load. Also, the wake development behind the downstream turbine was no longer axisymmetric. The tests were performed in a virtually turbulence free, uniform flow environment, as well as in a turbulent flow. In the latter case a grid was installed at the wind tunnel inlet producing a uniform inflow with about 10% turbulence intensity at the location of the upstream turbine. The results from the BT3 were reported in [3].

Motivation:

Given the constraints of transmission and installation costs, the available area for offshore wind farm installations is fairly limited. Under these circumstances, the wake effect plays a key role when evaluating the energy production since the energy captured by a wind turbine leads to a

decrease of the wind speed downstream. As a result, wind turbines located downstream produce less energy than if they were in the unobstructed free stream. In the case of onshore wind farms, the energy losses due to the wake effect constitute about 5 - 10% of the production [4], while in offshore wind farms, the wake effect losses can reach higher values; approximately 15% [5]. During the design stage of a wind farm, and in order to increase the wind farm production (by reducing wind speed deficits or wake effect losses), it would be desirable to separate the wind turbines as far as possible. However, due to constraints such as space availability and cost of electrical connections and the total cost of electrical losses over the lifespan of the installation the maximum distance between the individual wind turbines is limited [6].

The concept of individual power control of wind turbines was initially suggested by Steinbuch et al. [7] by selecting the tip speed ratio of each wind turbine by means of trial and error. In 2004, Corten and Schaak [8] presented experimental results showing the possibility of increasing the power generated and of reducing the loads by individually selecting the tip speed ratio of each wind turbine. In early 2011, Larsen et al. [9] presented the technical report corresponding to the TOPFARM project which deals with optimal topology design and control of wind farms. That study showed that it is possible to increase the overall efficiency of a wind farm through the individual control of the generated power by each wind turbine. In 2012 Lee et al. [10] presented a strategy of individual control of each of the wind turbines by optimizing the pitch angle of each turbine by means of a genetic algorithm, and used a wake model based on the eddy viscosity model. In that study, the authors considered the case of a row of wind turbines and achieved an improvement in the aerodynamic power of 4.5% with regard to the conventional operating strategy.

1 The BT4 test case definitions

BT4: In this fourth blind test we are focusing on the total power output from two in-line turbines. We use the same turbines as used in the previous BTs and study the influence of inlet conditions and turbine separation distance on the combined power performance of the two turbines.

The axial separation distance between the turbines is set $x/D = 2.77$, $x/D = 5.18$ and $x/D = 9.00$. Furthermore, we are able to provide three different inflow conditions at the inlet to the test section:

- **Low turbulence uniform inflow:** No grid at the inlet to the test section. At the position of the upstream turbine the turbulence intensity measured is $TI = 0.23\%$. The mean wind speed is uniform across the test section, apart from small wall boundary layer effects.
- **High turbulence uniform inflow:** An evenly spaced turbulence grid at the tunnel inlet generates a higher turbulence intensity level of $TI = 10.0\%$ at the location of the upstream turbine. The mean wind speed is uniform across the test section.
- **High turbulence shear inflow:** A turbulence grid with increasing vertical distance between the horizontal bars is installed at the inlet of the test section. This is creating a non-uniform shear flow with a mean turbulence intensity of $TI = 10.1\%$ over the rotor swept area of the upstream turbine.

In the following we provide detailed information about the setup of the different test cases. Depending on whether your computational model assumes axisymmetric flow and uses a rotating frame of reference, or computes a rotating rotor in a fixed environment, you may want to use the exact tunnel dimensions or convert the cross section to an equivalent circular cylinder in order to account for possible blockage effects and wall boundary layers. Furthermore, we provide full details of the model geometry. A CAD file that describes one blade mounted on one third of the nacelle is available. Alternatively, it is possible to build your own geometry from tables containing definitions of the airfoil, as

well as the chord length and twist as function of the radius. All information needed is described in the following sections.

1.1 The models

A picture of the turbine models installed in the wind tunnel is shown in *Figure 1*. Both turbines have three bladed upstream rotors with exactly the same blade geometry, but a slightly different total rotor diameter, due to different nacelle geometries. The blades were machined in aluminum and have a NREL S826 airfoil section from root to tip. (See: Somers [11] for the full airfoil documentation.)



Figure 1: Model wind turbines in the wind tunnel ($x/D=9.00$)

In *Figure 2* the dimensions of the two turbines are defined indicating that the models have slightly different tower and nacelle layouts. Note that the tower heights given in the figure show their physical dimensions to the fixing points below the wind tunnel floor and not their actual height as operated in the wind tunnel. These heights will be specified further down.

The upstream turbine will in the following be referred to as T_1 , while T_2 is defined to be the downstream turbine. The two turbines are positioned at three streamwise separation distances of $2.77D$, $5.18D$ and $9.00D$, where D is defined as $D = D_{T2} = 0.894m$. This is the diameter of the rotor of the downstream turbine T_2 .

The tower of turbine T_1 is a cylinder with a constant diameter of $D_{Tow,T1} = 0.11m$, while for T_2 the rotor sits on top of a stepped tower consisting of 4 cylinders of different diameters. T_2 is the same turbine that was used in BT1 [1]. The nacelle of turbine T_1 is a circular cylinder of $D_{Nac,T1} = 0.130m$ diameter. The nacelle of T_2 is also circular but with a diameter of $D_{Nac,T1} = 0.130m$. The rotor diameter of T_1 is $D_{T1} = 0.944m$, while $D_{T2} = 0.894m$. The individual blades have a total length of $l_{Blade} = 0.413m$ and are directly mounted on the hubs with the diameters $D_{hub,T1} = 0.118m$ and $D_{hub,T2} = 0.068m$.

Both turbines are driven by a belt transmission connected to a $0.37kW$ asynchronous motor located under the tunnel floor. Turbine T_1 has the belt mounted inside the tower, while for T_2 the tower is too slender to allow this, so the belt runs behind the turbine tower.

Turbine T_2 has an almost semi-spherical hub cover at the front. Its deviation from a sphere is small but if the exact geometry is deemed necessary, it may be obtained from the organizers as a table in an Excel file. In the CAD file mentioned above, the correct shape is of course included. At the rear, the cap is again formed from a sphere, slightly offset and with a somewhat larger diameter, as indicated in the figure. Turbine T_1 has a slightly pointed hub cover. The dimensions are documented in *Figure 2(a)*; a CAD file and an excel file are available for download for this turbine, too. Both turbines rotate in the counter-clockwise direction with the observer standing upstream and looking in flow direction.

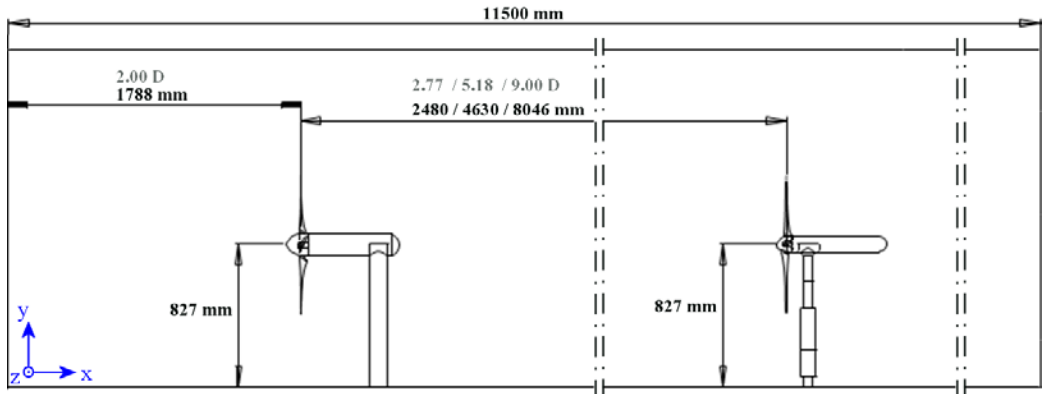


Figure 3: Turbine positions in the wind tunnel and reference coordinate system

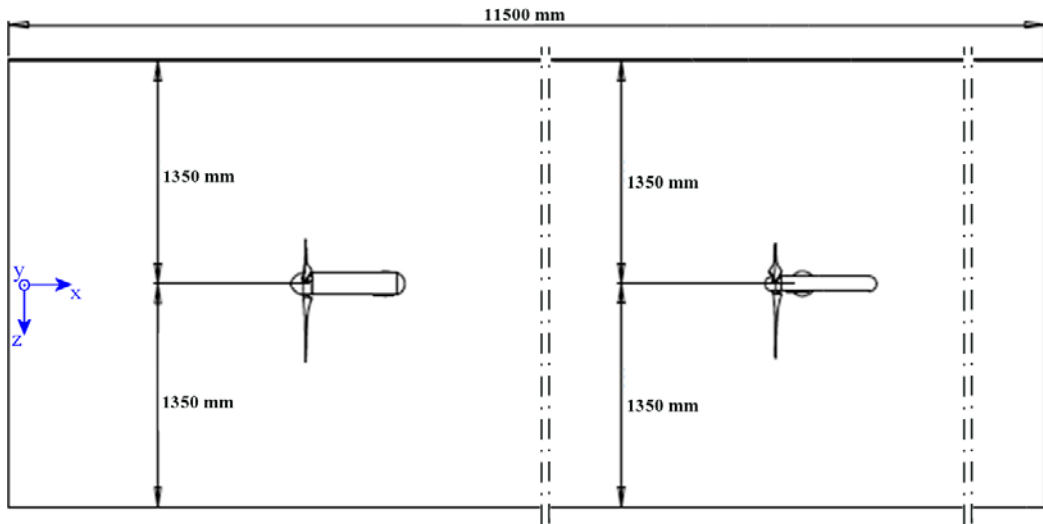


Figure 4: Wind tunnel test section from above and reference coordinate system

1.2 The blade geometry

The NREL S826 airfoil is used along the entire blade span. The normalized coordinates for the profile are given in Section 2. We also include a table of chord length and twist angle as function of the radius, which you will find in Section 3. Combined, this information allows you to define the blade geometry.

Furthermore, we supply a CAD file containing a 120 degrees segment of the nacelle of turbine T_2 with one blade mounted in the correct position as well as the complete 3D CAD files of both model turbines.

The CAD files may be downloaded from:

<http://www.ivt.ntnu.no/ept/downloads/workshop2015>

The login details are:

User: Workshop2015

Password: Turbine

1.3 The test environment

The model turbines were tested in a closed-return wind tunnel. It has a test section which is 2.71m wide and 11.15m long. The tunnel has a flexible roof which has been adjusted for zero pressure gradient at 10m/s. The tunnel heights are given in *Table 1*.

X (m)	Height (m)
0.000	1.801
2.810	1.801
5.621	1.813
8.435	1.842
11.150	1.851

Table 1: Height of test section as function of distance from the inlet

Both turbines were installed such that they have the same rotor axis height above the wind tunnel floor, $h_{hub} = 0.827m$ (see Figure 3).

All measurements were taken with a bulk velocity at the test section inlet equal to $U_\infty = 11.5m/s$. In the turbulent shear inflow case, the reference velocity at the rotor axis height $h_{hub} = 0.827m$ was set to $U_{ref,hub} = 11.5m/s$. The design tip speed ratio for both the upstream and downstream turbine is $\lambda = \Omega R/U_\infty = 6$. At the design condition this gives a Reynolds number of $Re_c = \lambda U c_{tip}/\nu \approx 10^5$, where c_{tip} is the chord length at the blade tip and ν the kinematic viscosity of air.

At the inlet to the empty test section the flow is uniform across the cross section to within $\pm 1\%$, except for the thin region of wall boundary layers, and the turbulence intensity was measured to be 0.23%. The conventional model which relates the dissipation rate of turbulent kinetic energy, E , to the streamwise velocity fluctuation, u , and the streamwise integral length scale, L_{uu} , is given by

$$E = \frac{3}{2} A \frac{u^3}{L_{uu}} \quad (1)$$

Using $\frac{3}{2}A \approx 1$ (taken from Krogstad and Davidson, [12]) the integral length in the streamwise direction at the test section inlet was calculated from measurements of u and E to be $L_{uu} = 0.035m$ when no grid was set up at the inlet. (Note that this length is virtually identical to the length scale obtained by integrating the streamwise auto-correlation function normally specified. However, this integral quantity is experimentally much harder to measure correctly and was therefore not used here.)

Test case A: Low turbulence (no grid):

At the position where the rotor center of the upstream turbine is located ($x/D = 2.00$, measured from the test section inlet), the length scale has slightly increased. At this axial position, the measurements give an integral length scale of $L_{uu} = 0.045 m$ and a turbulence intensity of $TI = 0.23\%$. Over the rotor swept area the mean velocity in the empty tunnel was found to be uniform to within $\pm 0.5\%$.

At the first axial position of the downstream turbine ($x/D = 2.00 + 2.77$), the turbulence intensity is again measured to be $TI = 0.23\%$ and the integral length scale is $L_{uu} = 0.053 m$.



Figure 5: Turbine models exposed to low turbulence inflow

Test case B: High turbulence (uniform turbulence grid):

In order to include the effects of atmospheric turbulence, the same measurements were performed using a large scale turbulence grid at the inlet to the test section. (See *Figure 6*) The bi-planar grid has a solidity of 35 % and is built from wooden bars of 47 mm x 47 mm cross-section. The grid mesh size was $M = 0.240m$, which at the position of the upstream turbine T_1 results in a turbulence intensity of $TI = 10.0\%$. The length scale here is estimated from equation (1) to be $L_{uu} = 0.065m$. This is a turbulent flow where the kinetic energy is decaying with the distance from the grid. Initially there are significant spanwise variations in the flow, but by the time the flow reaches the position of the upstream turbine, T_1 , the mean velocity is virtually independent of the spanwise coordinates and was found to be uniform to within $\pm 0.65\%$. Similarly, the turbulence intensity was constant to within $\pm 0.9\%$.

Since there are no significant spanwise variations in the flow, the kinetic energy dies out slowly downstream. As the flow reaches the first position of the downstream turbine ($x/D = 2.00 + 2.77$), the turbulence intensity in the empty tunnel drops to $TI = 4.8\%$ with a streamwise integral length scale of $L_{uu} = 0.100 m$.



Figure 6: Turbine models exposed to high turbulence inflow generated by an evenly spaced grid

Test case C: High turbulence shear flow (shear flow turbulence grid):

In a third test case the effect of shear flow in an atmospheric boundary layer combined with atmospheric turbulence is investigated. The same measurement series, as for the other test cases, were performed using a large scale shear flow turbulence grid at the inlet to the test section. (See *Figure 7*)



Figure 7: Turbine models exposed to highly turbulent shear flow

The horizontal mesh width is $0.240m$, while the vertical mesh heights vary between $0.0165m$ near the floor and $0.300 m$ underneath the roof. The grid is bi-planar and has a solidity of 38%. As for the evenly spaced turbulence grid, it is built from wooden bars of $47 mm \times 47 mm$ cross-section. The exact positions of the horizontal bars are documented in *Table 2*:

Bar no.	Height of bar center above the wind tunnel floor [mm]
8	1600
7	1300
6	1015
5	795
4	575
3	385
2	203
1	40

Table 2: Positions of the horizontal bars in the shear grid, measured at the bar center.

At the position of the upstream turbine, T_1 , a turbulence intensity of 10.1% is measured at the hub height. The turbulent length scale at the height of the nacelle $h=0.827m$ is estimated to be $L_{uu} = 0.097m$. The kinetic energy in the flow is decaying with the distance from the grid. At the first position of the downstream turbine ($x/D = 2.00 + 2.77$) the turbulence intensity has decayed to $TI = 5.2\%$ and the length scale has grown to $L_{uu} = 0.167m$. At the second downstream position ($x/D = 2.00 + 5.18$) a turbulence intensity of 4.1% and a $L_{uu} = 0.271m$ is measured. At the third downstream position ($x/D = 2.00 + 9.00$) the turbulence intensity has decayed to $TI = 3.7\%$ while the length scale has grown to $L_{uu} = 0.318m$.

As wind shear and turbulence are generated only at the grid position at the tunnel inlet, their development throughout the tunnel is measured at all four turbine positions. A common way to describe atmospheric wind shear is the power law, which expresses the wind speed, U , as function of height, z , provided that the wind speed at an arbitrary reference height, z_{ref} , is known:

$$\frac{U(z)}{U(z_{ref})} = \left(\frac{z}{z_{ref}} \right)^\alpha \quad (2)$$

The power law coefficient α describes the strength of shear in the wind profile. A wind profile based on a shear coefficient of $\alpha=0.11$ was chosen as a reference for this study, and the shear generating grid was designed to imitate this specific wind profile.

Figure 8 shows the mean wind speed, U , as function of the height z , as well as the turbulence intensity measured in the empty tunnel at the positions of the upstream turbine T_1 ($x_{T1} = 2.00D$) and the downstream turbine ($x_{T2,5D} = 2.00D + 2.77D \approx 5D$ // $x_{T2,7D} = 2.00D + 5.18D \approx 7D$ // $x_{T2,11D} = 2.00D + 9.00D \approx 11D$).

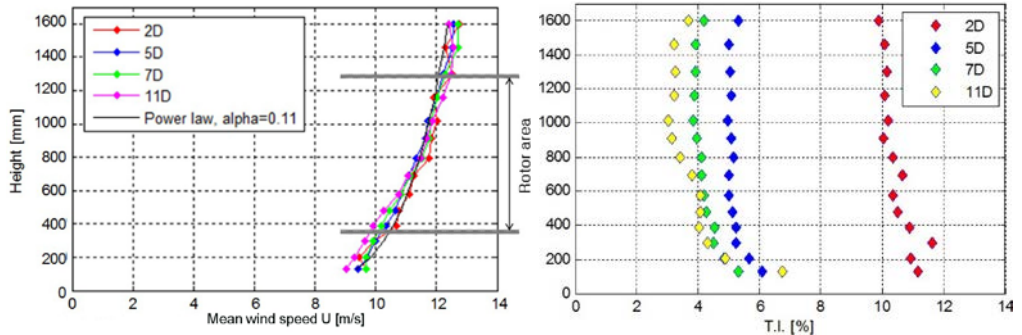


Figure 8: Measured mean wind speed and turbulence intensity at all measurement locations for turbulent shear inflow

2 Definition of the NREL S826 airfoil

The definitions of the NREL S826 airfoil used for the blade can be found in Somers [11] and the airfoil is shown in *Figure 9*. *Table 3* contains a list of the normalized coordinates for the airfoil. Somers specifies the geometry, as well as estimated performance characteristics, such as lift and drag coefficients, for a range of full scale operating Reynolds numbers. Unfortunately, these are computed for much higher Re than the ones applicable in the model tests.

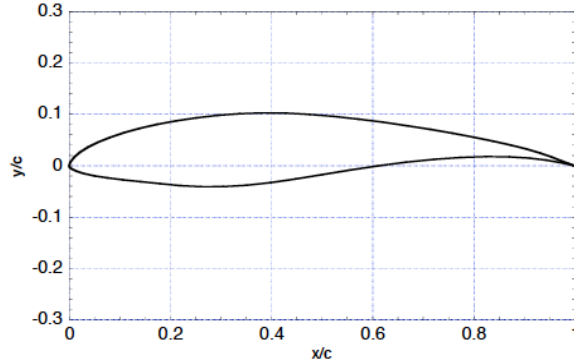


Figure 9: Shape of the NREL S826 airfoil

For the first two blind tests, the participants were asked to estimate the performance data for S826 themselves. When the predictions were analyzed and compared, we have seen that part of the scatter in the results may be traced back to the fact that different groups have generated quite different estimates for the lift and drag coefficients. We have decided to reduce the uncertainty of different airfoil coefficients and therefore provide a standard set of C_L and C_D coefficients that the participants should use for all operating conditions. Thus, some scatter in the predictions may disappear, possibly at the expense of introducing some systematic differences between the predictions and the measurements.

The data to be used is presented in *Table 4*. Note that this set is given for one Reynolds number only ($Re_c = 10^5$). This corresponds to the Re_c obtained at the blade tip at the design operating condition, i.e. at a tip speed ratio of 6. Obviously, this will be somewhat incorrect for the inner part of the blade, but the effects on the performance data at the design condition have been seen to be small.

In *Figure 10* the data from *Table 4* are compared with 2D measurements on the S826 performed at DTU, Denmark, [13] and at METUWIND, Turkey. The XFOIL data in *Table 4* are seen to fall between the measurements, capturing the trends from the METUWIND at the normal operating modes, but being closer to the DTU data at extremely high angles of attack. Measurements for $Re_c = 10^5$ are shown, but more data are available from both DTU's and the METUWIND's measurement campaigns.

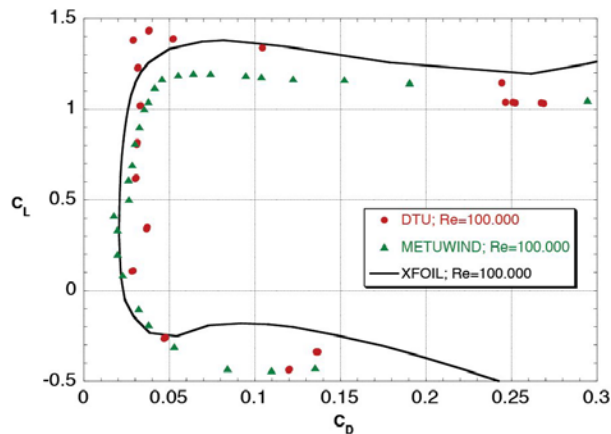


Figure 10: Comparison of C_L/C_D datasets [13]

If you are insisting on using lift and drag data at the correct Re as it varies with radial position and turbine operating conditions, you will need to generate your own data tables. You can do this by using the program package called *XFOIL* (see Drela [14]) or obtain the complete measurement data sets directly from DTU or METUWIND. (Contact information can be provided upon request.) It is important that you inform us about how the information is obtained if you do not use the data provided here.

x/c	y/c (upper surface)	x/c	y/c (lower surface)
0.0000	0.0000	0.0000	0.0000
0.00018000	0.0015900	0.00021000	-0.0014600
0.0025500	0.0074800	0.00093000	-0.0027400
0.0095400	0.016380	0.0021600	-0.0040300
0.020880	0.025960	0.0036700	-0.0052500
0.036510	0.035800	0.013670	-0.010350
0.056360	0.045620	0.029200	-0.015180
0.080260	0.055190	0.049980	-0.019600
0.10801	0.064340	0.075800	-0.023620
0.13934	0.072880	0.10637	-0.027290
0.17395	0.080680	0.14133	-0.030910
0.21146	0.087580	0.17965	-0.034860
0.25149	0.093430	0.21987	-0.038550
0.29361	0.098070	0.26153	-0.040640
0.33736	0.10133	0.30497	-0.040510
0.38228	0.10294	0.35027	-0.037940
0.42820	0.10249	0.39779	-0.032800
0.47526	0.10005	0.44785	-0.025630
0.52324	0.096070	0.50032	-0.017200
0.57161	0.090940	0.55484	-0.0084100
0.61980	0.084890	0.61055	-0.0001500
0.66724	0.078160	0.66644	0.0069900
0.71333	0.070950	0.72142	0.012540
0.75749	0.063410	0.77434	0.016210
0.79915	0.055720	0.82409	0.017840
0.83778	0.047980	0.86953	0.017410
0.87287	0.040290	0.90945	0.014980
0.90391	0.032620	0.94257	0.011130
0.93072	0.024790	0.96813	0.0068900
0.95355	0.016950	0.98604	0.0032400
0.97251	0.0098200	0.99655	0.0008400
0.98719	0.0043100	1.0000	0.0000
0.99668	0.0010300		
1.0000	0.0000		

Table 3: Coordinates for the NREL S826 airfoil

α	C_L	C_D	C_L/C_D	α	C_L	C_D	C_L/C_D
-40.0	-0.96710	0.39968	-2.4197	3.00	0.82540	0.023250	35.501
-35.0	-0.87580	0.36549	-2.3962	4.00	0.91800	0.024420	37.592
-30.0	-0.75170	0.32383	-2.3213	5.00	1.0019	0.025880	38.713
-25.0	-0.60080	0.27557	-2.1802	6.00	1.0783	0.027800	38.788
-20.0	-0.43470	0.22170	-1.9608	7.00	1.1469	0.030290	37.864
-18.0	-0.36800	0.19869	-1.8521	8.00	1.2060	0.033540	35.957
-16.0	-0.30430	0.17474	-1.7414	9.00	1.2550	0.037850	33.157
-14.0	-0.24910	0.14843	-1.6782	10.0	1.2929	0.043660	29.613
-12.0	-0.20180	0.12244	-1.6482	11.0	1.3320	0.049960	26.661
-11.0	-0.18650	0.10792	-1.7281	12.0	1.3509	0.059220	22.812
-10.0	-0.18110	0.091970	-1.9691	13.0	1.3718	0.069050	19.867
-9.00	-0.19240	0.073190	-2.6288	14.0	1.3784	0.081720	16.867
-8.00	-0.25200	0.054460	-4.6272	15.0	1.3638	0.098800	13.804
-7.00	-0.23440	0.038600	-6.0725	16.0	1.3431	0.11883	11.303
-6.00	-0.14360	0.029050	-4.9432	18.0	1.2563	0.17904	7.0169
-5.00	-0.049500	0.023940	-2.0677	20.0	1.1940	0.26157	4.5647
-4.00	0.071400	0.021820	3.2722	22.0	1.2493	0.29458	4.2410
-3.00	0.18800	0.021090	8.9142	25.0	1.3379	0.33390	4.0069
-2.00	0.30260	0.020730	14.597	30.0	1.4702	0.38800	3.7892
-1.00	0.41360	0.020770	19.913	34.0	1.5519	0.42331	3.6661
0.00	0.52200	0.021040	24.810	40.0	0.96620	0.63129	1.5305
1.00	0.62690	0.021530	29.118	50.0	0.84970	0.73405	1.1576
2.00	0.72880	0.022220	32.799				

Table 4: Lift and drag coefficients calculated for $Re = 1.0 \times 10^5$ using *XFOIL*.

3 Chord and twist data

Table 5 contains a list of the airfoil chord length and twist angle as function of the radius. (The twist angle is measured with respect to the rotor plane.) Please note that for the first 3 coordinate sets the geometry consists of a circular cylinder used to fix the blade to the hub. Therefore a major part of this section is located inside the hub when defining the rotor geometry. This section has been identified in the table by setting the twist angle to 120 degrees. Between the last circular section and the first NREL profile, a linear transition region is giving a smooth change of shape. The blade is shown in Figure 11.

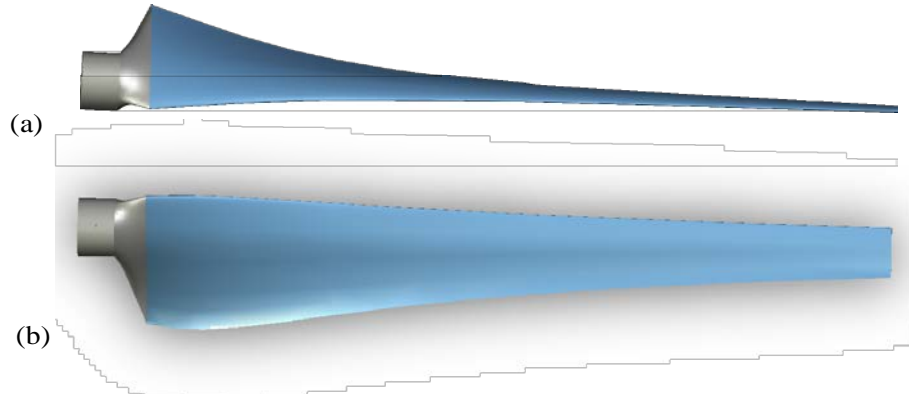


Figure 11: Blade (a) seen in the plane of rotation and (b) in the axial direction

Figure	c (m)	φ (deg)
0.0075000	0.013500	120.00
0.022500	0.013500	120.00
0.049000	0.013500	120.00
0.055000	0.049500	38.000
0.067500	0.081433	37.055
0.082500	0.080111	32.544
0.097500	0.077012	28.677
0.11250	0.073126	25.262
0.12750	0.069008	22.430
0.14250	0.064952	19.988
0.15750	0.061102	18.034
0.17250	0.057520	16.349
0.18750	0.054223	14.663
0.20250	0.051204	13.067
0.21750	0.048447	11.829
0.23250	0.045931	10.753
0.24750	0.043632	9.8177
0.26250	0.041529	8.8827
0.27750	0.039601	7.9877
0.29250	0.037831	7.2527
0.30750	0.036201	6.5650
0.32250	0.034697	5.9187
0.33750	0.033306	5.3045
0.35250	0.032017	4.7185
0.36750	0.030819	4.1316
0.38250	0.029704	3.5439
0.39750	0.028664	2.9433
0.41250	0.027691	2.2185
0.42750	0.026780	1.0970
0.44250	0.025926	-0.7167

Table 5: Definitions of chord length and twist angle as function of blade radius.

4 Operating conditions

This section describes the operating configurations for which the computational output may be submitted. For all cases the upstream turbine T_1 is located at $x = 1788\text{mm}$ measured from the inlet to the test section, which corresponds to a distance of $2.00D$.

For the test cases **A**, **B** and **C** the downstream turbine T_2 is positioned at $\Delta x = 4630\text{mm}$ behind the upstream turbine, which corresponds to $5.18D$ separation distance. The inflow conditions are varied from low turbulence (**A**), to high turbulence (**B**) and high turbulence shear flow (**C**).

For the test cases **B₁**, **B₂**, **B₃**, the inflow condition is set to high turbulence (**B**) and is not varied. However, here the streamwise separation distance between the turbines is varied from $\Delta x = 2480\text{mm}$ ($2.77D$, **B₁**) through $\Delta x = 4630\text{mm}$ ($5.18D$, **B₂**) to $\Delta x = 8046\text{mm}$ ($9.00D$, **B₃**).

This comparison should illustrate the influence of the separation distance on the total efficiency.

This makes up a total number of **5 test cases** as test case **B** and **B₂** are identical. For all test cases the inflow velocity is set to $U_\infty = 11.5\text{m/s}$; for the non-uniform shear inflow (test case **C**) this is the reference inflow velocity at hub height $h_{hub} = 0,827\text{m}$. The blade pitch angle is set to $\beta = 0^\circ$ for all test cases. The density of air can be assumed to be $\rho = 1.20\text{kg/m}^3$.

4.1 Test cases A, B, C: varying inflow conditions

For these test cases the downstream turbine's position is fixed at $\Delta x = 4630\text{mm}$ ($5.18D$) behind the upstream turbine. The inflow conditions are varied from **low turbulence (A)**, to **high turbulence (B)** and **high turbulence shear flow (C)**. A detailed description of the inflow conditions is given in section 3.

4.1.1 Turbine performance C_p and thrust C_T :

The **upstream turbine** T_1 is operated at a tip speed ratio of $\lambda_{T1} = \Omega R/U_\infty = \mathbf{6.0}$, whereas the **downstream turbine** T_2 is run at $\lambda_{T2} = \Omega R/U_\infty = \mathbf{4.5}$. Note, that the same reference velocity U_∞ is used for both turbines.

For each inlet condition **A**, **B** and **C**,

1. the **power coefficients** $C_{p,T1}$ and $C_{p,T2}$ as well as
2. the **thrust coefficients** $C_{T,T1}$ and $C_{T,T2}$

should be presented at these operating points.

The thrust coefficients should be calculated for the rotor only, i.e. the contribution of the tower to the thrust must not be taken into account.

4.1.2 Horizontal wake profiles

Furthermore, the horizontal wake profile at $\Delta x = 2480\text{mm}$ ($2.77D$) behind the **upstream turbine** T_1 should be documented at $\lambda_{T1} = \mathbf{6.0}$ for the three inlet conditions **A**, **B** and **C**. This is an axial position in between the two turbines.

A profile of the

1. **normalized mean velocity** U/U_∞ as well as the
2. **normalized turbulent kinetic energy** $k^* = k/U_\infty$

should be presented. Profiles along a horizontal line at the elevation of the center of the turbine hub ($h_{hub} = 0.827\text{ m}$) should be extracted covering the horizontal span width from $z = -944\text{mm}$ ($-2 R_{T1}$) to $z = +944\text{mm}$ ($+2 R_{T1}$). For the reference coordinate system, see *Figure 3* and *Figure 4*.

4.2 Test cases **B**₁, **B**₂, **B**₃: varying turbine separation distance

For this test case comparison the large scale turbulence grid is placed at the inlet to the test section (Inlet condition **B**). In these calculations the turbulence intensity at the position of the upstream turbine T_1 should be adjusted to be $TI = 10.0\%$. See section 1.3 for integral length scales as well as the axial development of the turbulence intensity through the tunnel.

In this comparison the streamwise separation distance between the two turbines is varied from $\Delta x = 2480\text{mm}$ ($2.77D$, test case **B**₁) to $\Delta x = 4630\text{mm}$ ($5.18D$, test case **B**₂) and up to $\Delta x = 8046\text{mm}$ ($9.00D$, test case **B**₃). Thus, the influence of the separation distance on the total efficiency will be illustrated.

4.2.1 Turbine performance C_P and thrust C_T

The **upstream turbine** T_1 is operated at a tip speed ratio of $\lambda_{T1} = 6.0$, whereas the tip speed ratio of the **downstream turbine** T_2 is fixed to $\lambda_{T2} = 4.5$.

For each axial separation distance $2.77D$, $5.18D$ and $9.00D$

3. the **power coefficient** $C_{P,T2}$ as well as
4. the **thrust coefficient** $C_{T,T2}$

should be presented at the given operating points. The coefficients $C_{P,T1}$ and $C_{T,T1}$ for T_1 have already been calculated previously in test case **B**.

4.2.2 Horizontal wake profiles

Also for this test series, three horizontal wake profiles behind the **upstream turbine** T_1 run at $\lambda_{T1} = 6.0$ at $\Delta x = 2480\text{mm}$ (**2.77D**) to $\Delta x = 4630\text{mm}$ (**5.18D**) and up to $\Delta x = 7600\text{mm}$ (**8.50D**) should be extracted from test case **B**₃ (separation distance $x/D = 9.00$).

A profile of the

1. **normalized mean velocity** U/U_∞ as well as the
2. **normalized turbulent kinetic energy** $k^* = k/U_\infty$

should be presented. Profiles along a horizontal line at the elevation of the center of the turbine hub ($h_{hub} = 0.827\text{ m}$) should be extracted covering the horizontal span width from $z = -944\text{mm}$ ($-2 R_{T1}$) to $z = +944\text{mm}$ ($+2 R_{T1}$).

5 Computation output

The main aim of this blind test is to find out how well the performance of a turbine operated at different inlet conditions and different separation distances are predicted. Therefore the most important outputs are the C_P and C_T values of the downstream turbine.

The operating conditions for the turbines should be set to a free stream velocity of $U_\infty = 11.5\text{m/s}$. The same reference velocity should be used for both turbines when scaling the output, even though the downstream turbine will experience a different reference velocity than the upstream turbine due to the reduced velocity in the wake of the upstream turbine. A data template is provided to ensure that data from all participants can be presented in the same way.

Test cases A, B, C and B₁, B₂, B₃:

The participants are requested to provide the following output:

1. The power coefficient $C_p = 2P/\rho U_\infty^3 A$ and the thrust coefficient $C_T = 2T/\rho U_\infty^2 A$ at $\lambda_{T1} = 6.0$ for the **upstream turbine**. Here P is the power extracted from the wind, T is the force acting on the rotor plane in the direction of the wind and A is the rotor swept area ($A = \pi D^2/4$). Please note that the drag of the tower and the nacelle must NOT be included in C_T .
2. The power coefficient $C_p = 2P/\rho U_\infty^3 A$ and the thrust coefficient $C_T = 2T/\rho U_\infty^2 A$ for the **downstream turbine**. For test cases A, B and C the downstream turbine tip speed ratio is set to $\lambda_{T2} = 4.5$. For the test cases B₁, B₂ and B₃ λ_{T2} varies with increasing turbine separation distance: $\lambda_{T2,B1} = 4.0$, $\lambda_{T2,B2} = 4.5$, $\lambda_{T2,B3} = 5.0$. Test case B and test case B2 are identical. Again, the drag of the tower and nacelle must NOT be included in C_T .
3. The non-dimensional streamwise mean velocity U/U_∞ along a horizontal line in z -direction at hub height $y = h_{hub} = 0.827m$. For test cases A, B and C the mean velocity profile should be extracted at $\Delta x = 2480mm$ ($2.77D$) behind the **upstream turbine** rotor when T_1 is operated at $\lambda_{T1} = 6.0$. Additionally, the mean velocity profile should be extracted from test case B₃ at $\Delta x = 2480mm$ ($2.77D$), $\Delta x = 4630mm$ ($5.18D$) as well as $\Delta x = 7600mm$ ($8.50D$) downstream of the upstream turbine rotor. The profiles should cover the horizontal span width from $z = -944mm$ ($-2 R_{T1}$) to $z = +944mm$ ($+2 R_{T1}$). For a reference coordinate system, see *Figure 3* and *Figure 4*.
4. The normalized turbulent kinetic energy $k^* = k/U_\infty^2$ along the same horizontal lines. For test case A, B and C at $\Delta x = 2480mm$ ($2.77D$) downstream of T_1 , for the test case B₃ at $\Delta x = 2480mm/4630mm/7600mm$ behind the **upstream turbine** rotor. The turbulent kinetic energy is defined as $k = \frac{1}{2}(u_x^2 + u_r^2 + u_\theta^2)$ in a cylindrical coordinate system, or you might use a corresponding approximation.
5. A detailed description of the computational method you are using. This should give us all important information to allow us to classify your method and group the results according to the methods used.
We require the name and type of the numerical code or software you are using and the turbulence model that is used. It should be described how the rotor is modelled (fully resolved rotor, Blade Element Momentum method, actuator disc method, actuator line method,...). Important parameters describing the computational mesh, such as resolution, number of cells and frame of reference should be provided. Moreover, it should be clarified how the inflow condition is modelled, i.e. if you resolve the turbulence grids or set specific initial conditions to the domain.
Furthermore, it is important that you state the source for the lift and drag coefficients you used for the calculation of the lift and drag forces on the rotors. Finally, it is important to mention which structures and boundaries (wind tunnel walls, turbine towers and nacelles,...) have been taken into account for in the simulations.

References

- [1] Krogstad P.-Å., Eriksen P.E.; "Blind test" calculations of the performance and wake development for a model wind turbine. *Renewable Energy*. vol. 50., 2013
- [2] Pierella F., Krogstad P.-Å., Sætran L.R.; Blind Test 2 calculations for two in-line model wind turbines where the downstream turbine operates at various rotational speeds. *Renewable Energy*. vol. 70., 2014
- [3] Krogstad P.-Å., Sætran L.R., Adaramola M.S.; "Blind Test 3" calculations of the performance and wake development behind two in-line and offset model wind turbines. *Journal of Fluids and Structures*. vol. 52., 2014
- [4] Krohn S., Morthorst P.E.; Awerbuch S.; The economics of wind energy. European Wind Energy Assosiation, 2009. Available at: http://www.ewea.org/fileadmin/files/library/publications/reports/Economics_of_Wind_Energy.pdf [accessed on 10.03.2015].
- [5] Barthelmie R., Larsen G., Frandsen S., Folkerts L., Rados K., Pryor S., Lange B.; Schepers G.; Comparison of wake model simulations with offshore wind turbine wake profiles measured by SODAR, *J.Atmos.Ocean.Technol.*, 2006
- [6] Serrano González J., Burgos Payán M., Riquelme Santos J.; Optimum design of transmissions systems for offshore wind farms including decision making under risk, *Renewable Energy*, 2013
- [7] Steinbuch M., de Boer W., Bosgra O., Peters S., Ploeg J.; Optimal control of wind power plants, *J. Wind Eng. Ind. Aerodyn.* 1988
- [8] Corten G., Schaak P., Bot E., More Power and Less Loads in Wind Farms: 'Heat and Flux'; European Wind Energy Conference & Exhibition, 2004
- [9] Larsen G.C., Aagaard Madsen H., Troldborg N., Larsen T.J., Réthoré P., Fuglsang P.; TOPFARM-next generation design tool for optimisation of wind farm topology and operation, 2011
- [10] Lee J., Son E., Hwang B., Lee S.; Blade pitch angle control for aerodynamic performance optimization of a wind farm, *Renewable Energy*, 2012
- [11] Somers D.M.; The S825 and S826 Airfoils. *National Renewable Energy Laboratory*; NREL/SR-500-36344, 2005
- [12] Krogstad P.-Å., Davidson P.A.; Is grid turbulence Saffman turbulence? *J. Fluid Mech.* 642, 2010
- [13] Sarmast S., Mikkelsen R.F.; The experimental results of the NREL S826 Airfoil at low Reynolds numbers DTU, Lyngby, Denmark, 2013
- [14] Drela M.; XFOIL Subsonic Airfoil Development System; available at: <http://web.mit.edu/drela/Public/web/xfoil/> [accessed on 20.03.2015]